J. Math. Biol. (2016) 73:1823–1849
DOI 10.1007/s00285-016-1011-7

Mathematical Biology

# Uncertainty quantification in flux balance analysis of spatially lumped and distributed models of neuron–astrocyte metabolism

**Daniela Calvetti**[1] · **Yougan Cheng**[2] · **Erkki Somersalo**[1]

Received: 11 November 2014 / Revised: 11 April 2016 / Published online: 5 May 2016


**Abstract** Identifying feasible steady state solutions of a brain energy metabolism model is an inverse problem that allows infinitely many solutions. The characterization of the non-uniqueness, or the uncertainty quantification of the flux balance analysis, is tantamount to identifying the degrees of freedom of the solution. The degrees of freedom of multi-compartment mathematical models for energy metabolism of a neuron–astrocyte complex may offer a key to understand the different ways in which the energetic needs of the brain are met. In this paper we study the uncertainty in the solution, using techniques of linear algebra to identify the degrees of freedom in a lumped model, and Markov chain Monte Carlo methods in its extension to a spatially distributed case. The interpretation of the degrees of freedom in metabolic terms, more specifically, glucose and oxygen partitioning, is then leveraged to derive constraints on the free parameters to guarantee that the model is energetically feasible. We demonstrate how the model can be used to estimate the stoichiometric energy needs of the cells as well as the household energy based on the measured oxidative cerebral metabolic rate of glucose and glutamate cycling. Moreover, our analysis shows that in the lumped model the net direction of lactate dehydrogenase (LDH) in the cells can be deduced from the glucose partitioning between the compartments. The extension

The work of Daniela Calvetti was partly supported by Grant Number 246665 from the Simons Foundation, and the work of Erkki Somersalo was partly supported by NSF Grant DMS 1016183. Daniela Calvetti and Erkki Somersalo were partly supported by NIH, grant 1U01GM111251-01.

✉ Daniela Calvetti
dxc57@case.edu

[1] Department of Mathematics, Applied Mathematics and Statistics, Case Western Reserve University, 10900 Euclid Avenue, Cleveland, OH 44106, USA

[2] School of Mathematics, University of Minnesota, 206 Church St SE, Minneapolis, MN 55455, USA

of the lumped model to a spatially distributed multi-compartment setting that includes diffusion fluxes from capillary to tissue increases the number of degrees of freedom, requiring the use of statistical sampling techniques. The analysis of the distributed model reveals that some of the conclusions valid for the spatially lumped model, e.g., concerning the LDH activity and glucose partitioning, may no longer hold.

**Keywords** Brain energy metabolism · Bayesian flux balance analysis · Lactate shuttle · Distributed model · Glucose partitioning

**Mathematics Subject Classification** 92C20 Neural biology · 92C40 Biochemistry · 92B05 Biomathematics · 62F15 Bayesian inference

## 1 Introduction

Energy metabolism in human brain depends on a complex metabolic network comprising the biochemical reactions occurring in tissue, and the exchanges of metabolic substrates and byproducts between tissue and capillaries. The difficulty of directly measuring quantities of interest in humans without disrupting the brain functions underlines the need for detailed mathematical models that provide a connection between the quantities of primary interest and the observed ones. Mathematical models of progressively increasing sophistication have been proposed over the past decade, see, e.g., Aubert and Costalat (2005), Calvetti and Somersalo (2011, 2013), Cloutier et al. (2009), Nuzzo et al. (2010), Simpson et al. (2007).

In steady state analysis, or flux balance analysis, of a metabolic network, it is assumed that the concentrations of metabolites and intermediates are constant, and the objective is to look for configurations of reaction fluxes and cross-membrane transport rates that can maintain the brain in a given state. In mathematical terms, the analysis of a steady state model, governed by systems of linear equations with constraints on some of the unknowns, aims at estimating the activity level of the various reactions and transports, while providing no information about the concentrations of the biochemical species.

Kinetic metabolic models, on the other hand, whose aim is to describe the time courses of the different metabolite and intermediate concentrations, are governed by systems of differential equations depending on a large number of parameters whose values are either unknown or poorly known. A standard method for estimating the unknown model parameters is to fit the model predictions to measured concentration data using a reliable numerical method. The underlying parameter estimation problem for detailed models that depend on a large number of unknown parameters may be challenging because of the limited amount of available data, which, in addition, often come from a cohort of subjects, thus introducing an intrinsic model discrepancy. A possible alternative would be to use parameter values deduced indirectly from in vitro measurements of quantities which may include the density of membrane transporters or enzyme expression levels. In addition to the difficulty of obtaining such measurements, the passage from this kind of data to model parameters is not at all straightforward, in particular because the connection between the cellular level measurements and the

lumped macroscopic model parameters is poorly understood (Calvetti and Somersalo 2015).

In both types of models, the quest for information about the unobservable quantities can be cast as an inverse problem. Indeed, the problem is ill-posed: usually it does not have a unique solution, and the possible solutions are sensitive to uncertainties both about the model and the data. Non-uniqueness of the solution in the case of biological systems often is a reflection of an intrinsic and important property of living systems that are able to adapt to changing external conditions not included in the model, as is the case in anomalous and diseased states. In this light, computational methods that, instead of identifying a single solution, proceed to characterize all possible states that are viable under given limitations are of importance. In the context of inverse problems, the statistical framework is the natural environment to pass from single anecdotal solutions to a description of the full set of possible solutions with respective probabilities (Calvetti and Somersalo 2007). Recasting inverse problems as statistical inference problems has become a rather widespread practice in the field of uncertainty quantification of complex systems.

In this article, we address uncertainty quantification for metabolic flux balance analysis. We consider first a strongly reduced spatially lumped metabolic model of a neuron/astrocyte complex, showing that the model admits two degrees of freedom that completely determine the system. In particular, the model uncertainty can be fully characterized in a two-dimensional space, and various implications such as the direction of lactate transport between the cells can be described in terms of the degrees of freedom that, in turn, can be interpreted in physiological terms. Moreover, the analysis of the simple model allows us to infer about the energetic cost of the neurotransmitter cycling between neurons and astrocytes.

A more complex model is constructed by putting together a line of neuron–astrocyte units to model a spatially distributed system. While, in principle, the degrees of freedom of this system can still be extracted analytically, the visualization and extraction of information about the multidimensional set of possible solutions calls for more sophisticated tools. In our example we resort to statistical sampling methods, and in particular, Markov chain Monte Carlo (MCMC) methods. We show that while some of the conclusions drawn from the simple model remain valid, the spatial distribution and the increased dimensionality of the problem add a significant degree of uncertainty.

## 2 Single unit: a simplified neuron–astrocyte complex

In this section, we consider a simplified, spatially lumped compartment model for neuron–astrocyte interactions during neurotransmitter cycling. We show that the model has two degrees of freedom, and they can be described in terms of glucose and oxygen partitioning between the neuron and the astrocyte. In order for the model to be physiologically meaningful, the metabolic flux configuration must be able to meet the aggregate energetic needs of the complex, which comprise the cost for performing basic household chores and the energy required to support the signaling activities. This, in turn, translates into a set of constraints for the reaction fluxes and transport rates, which will be derived starting from the underlying physiological motivations.

### 2.1 Stoichiometry and degrees of freedom

Consider a simplified mathematical model of a neuron–astrocyte complex, equipped with the transports of glucose, lactate, oxygen and carbon dioxide between blood, extracellular space (ECS) and the cell compartments comprising, in each cell type, a lumped glycolysis, lactate dehydrogenase (LDH), integrated pyruvate dehydrogenase (PDH) and tricarboxylic acid (TCA) cycle, and oxidative phosphorylation (OxPhos). Furthermore, we assume that the two cell types are coupled through a glutamate-glutamine cycling over the synaptic cleft: we refer to the neurotransmitter cycle as the V-cycle.

The energetic needs for keeping the glutamatergic signaling active at steady rate are different for neuron and astrocyte. In the neuron, the energetic cost can be attributed mainly to three types of tasks: (a) presynaptic activities including sodium–calcium exchange and glutamate packing in vesicles; (b) post-synaptic cost consisting mostly of the energy needed for the sodium–potassium pumps as well as sodium–calcium exchange; (c) action potential propagation to trigger synaptic signaling where energy is required for repolarization of the membrane. In astrocyte, energy is needed for glutamate uptake and glutamine synthetase. Moreover, astrocytes have other energy-demanding tasks indirectly related to the synaptic signaling, such as potassium cleaning. We refer to Attwell and Laughlin (2001), Harris et al. (2012), Howarth et al. (2012) for more detailed discussions of the mechanisms.

To include the energetic cost in the model, we let $E_{\mathrm{n}}$ and $E_{\mathrm{a}}$ denote the stoichiometric energy cost in neuron and astrocyte, respectively. More precisely, $E_{\mathrm{n}}$ ($E_{\mathrm{a}}$) is the number of ATP molecules needed in neuron (astrocyte) to cycle one molecule of glutamate through the V-cycle. We will discuss the values of $E_{\mathrm{n}}$ and $E_{\mathrm{a}}$ in detail later on. To implement the energetic cost into the model in a stoichiometric manner without increasing its complexity excessively, e.g., by including the transmembrane ion fluxes as new unknowns, we bundle the energy consumption of the transmitter cycle with

**Table 1** List of the lumped reactions included in the model

| Neuron | Astrocyte | Reaction |
|---|---|---|
| $\varphi_1$ | $\varphi_7$ | $\mathrm{Glc} + 2\,\mathrm{NAD}^+ + 2\,\mathrm{ADP} \longrightarrow 2\,\mathrm{Pyr} + 2\,\mathrm{NADH} + 2\,\mathrm{ATP}$ |
| $\varphi_2$ | $\varphi_8$ | $\mathrm{Pyr} + \mathrm{NADH} \longrightarrow \mathrm{Lac} + \mathrm{NAD}^+$ |
| $\varphi_3$ | $\varphi_9$ | $\mathrm{Pyr} + \mathrm{ADP} + 5\,\mathrm{NAD}^+ \longrightarrow 3\,\mathrm{CO}_2 + \mathrm{ATP} + 5\,\mathrm{NADH}$ |
| $\varphi_4$ | $\varphi_{10}$ | $\mathrm{O}_2 + 2\mathrm{NADH} + 5\mathrm{ADP} \longrightarrow 2\,\mathrm{NAD}^+ + 5\,\mathrm{ATP} + 2\,\mathrm{H}_2\mathrm{O}$ |
| $\varphi_5$ | – | $\mathrm{Gln} + E_n\,\mathrm{ATP} \longrightarrow \mathrm{Glu} + E_n\,\mathrm{ADP}$ |
| – | $\varphi_{11}$ | $\mathrm{Glu} + E_a\,\mathrm{ATP} \longrightarrow \mathrm{Gln} + E_a\,\mathrm{ADP}$ |
| $\varphi_6$ | $\varphi_{12}$ | $\mathrm{ATP} \rightarrow \mathrm{ADP}$ |

The phosphate activated glutaminase (PAG), or $\varphi_5$, accounts for the total neuronal energetic need required to maintain the steady state glutamine/glutamate cycle. The energetic need $E_n$ will be specified in the computed examples. Similarly, $\varphi_{11}$ in astrocyte, representing the glutamine synthetase (GS), accounts for the astrocytic energetic need, defined by $E_a$. The ATP dehydrogenase reactions, $\varphi_6$ and $\varphi_{12}$, account for non-specific energy consuming processes in the cells. All the reactions except for lactate dehydrogenase (LDH), denoted by $\varphi_2$ in neuron and $\varphi_8$ in astrocyte, are unidirectional

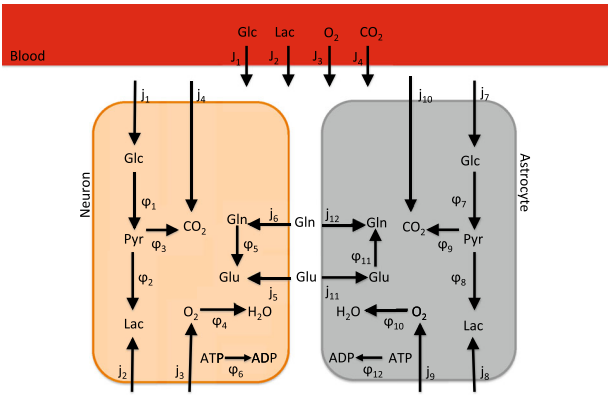


**Fig. 1** The pathway chart and compartment configuration of the model considered in the simplified metabolic network. The *arrows* in the diagram indicate the direction of the flux with a positive sign, which may not be the preferred direction. The ATP/ADP and NADH/$NAD^+$ dynamics are not indicated in the figure

the V-cycle reactions phosphate activated glutaminase (PAG) in neuron and glutamine synthetase (GS) in astrocyte. The lumped reactions included in this model are listed in Table 1, and the metabolic network is illustrated schematically in Fig. 1. Observe that in Table 1, we list the ATP hydrolysis, with fluxes $\varphi_6$ and $\varphi_{12}$ in neuron and astrocyte, as separate reactions. These fluxes are related to the household energetic needs of the cells, which are independent of the V-cycle activity level. The household energy and its implementation into the model will be discussed in detail later on.

We denote by $\mathbf{J} = [J_1; J_2; J_3] \in \mathbb{R}^3$ the column vector of the aggregated tissue uptake of glucose, lactate and oxygen, respectively, from the capillary blood, with the sign convention that $J_j > 0$ indicates transport into the tissue. The ratio of oxygen to glucose uptake, referred to as the oxygen glucose index, OGI, is defined by

$$\mathrm{OGI} = \frac{J_3}{J_1}.$$

It follows from the stoichiometry that the complete oxidation of glucose in tissue,

$$\mathrm{C_6H_{12}O_6} + 6\,\mathrm{O_2} \rightarrow 6\,\mathrm{CO_2} + 6\,\mathrm{H_2O},$$

requires that OGI = 6: an OGI smaller than 6 indicates the presence of non-oxidative metabolism, or production of lactate, while an OGI greater than 6 signals the oxidation of substrates other than glucose, which in the present model are limited to lactate. The balance equation including the lactic acid ($\mathrm{C_3H_6O_3}$) is

$$\mathrm{C_6H_{12}O_6} + \mathrm{OGI} \times \mathrm{O_2} \rightarrow \left(2 - \frac{\mathrm{OGI}}{3}\right) \times \mathrm{C_3H_6O_3} + \mathrm{OGI} \times \mathrm{CO_2} + \mathrm{OGI} \times \mathrm{H_2O}. \quad (1)$$

**Table 2** Stoichiometric relations between the reaction and transport rates that follow from balancing the concentrations of the indicated species in each compartment

| Species | Neuron | Astrocyte | ECS |
|---|---|---|---|
| Pyr | $2\varphi_1 - \varphi_2 - \varphi_3 = 0$ | $2\varphi_7 - \varphi_8 - \varphi_9 = 0$ | – |
| ATP | $2\varphi_1 + \varphi_3 + 5\varphi_4 - E_n\varphi_5 - \varphi_6 = 0$ | $2\varphi_7 + \varphi_9 + 5\varphi_{10} - E_a\varphi_{11} - \varphi_{12} = 0$ | – |
| NADH | $2\varphi_1 - \varphi_2 + 5\varphi_3 - 2\varphi_4 = 0$ | $2\varphi_7 - \varphi_8 + 5\varphi_9 - 2\varphi_{10} = 0$ | – |
| Glu | see Table 3 | see Table 3 | $j_5 = -j_{11}$ |
| Gln | see Table 3 | see Table 3 | $j_6 = -j_{12}$ |

We remark that the coefficient of lactic acid may become negative when OGI >6, indicating uptake, rather than release, of this metabolite.

Consider the reductive/oxidative reactions $\varphi_1, \ldots, \varphi_4$ in the neuron, listed in Table 1. By subtracting side by side the pyruvate balance equation and the NADH balance equation given in Table 2, we obtain

$$6\varphi_3 - 2\varphi_4 = 0 \quad \text{or} \quad 3\varphi_3 = \varphi_4. \tag{2}$$

Solving for $\varphi_3$ and substituting the result in the pyruvate balance equation yields

$$6\varphi_1 - 3\varphi_2 - \varphi_4 = 0. \tag{3}$$

Repeating the same procedure for astrocyte, we have that

$$6\varphi_7 - 3\varphi_8 - \varphi_{10} = 0. \tag{4}$$

Equation 2, together with the stoichiometric relations $j_3 = \varphi_4$ and $j_4 = -3\varphi_3$, see Table 3, implies that $j_4 = -j_3$, that is, the carbon dioxide efflux rate equals that of oxygen influx in neuron. The same holds in astrocyte, thus implying that $J_4 = -J_3$ as already indicated in (1). In the light of these observations, it suffices to consider the transfer of glucose, lactate, and oxygen.

Let $\mathbf{j}^n = [j_1; j_2; j_3]$ be the column vector whose entries are the uptake rates of glucose, lactate and oxygen, respectively, in neuron, and $\mathbf{j}^a = [j_7; j_8; j_9]$ the corresponding rate vector in astrocyte. From the convention that a positive flux goes from the ECS into the cell and the fact that, at steady state, the equalities $[j_1; j_2; j_3] = [\varphi_1; -\varphi_2; \varphi_4]$ and $[j_7; j_8; j_9] = [\varphi_7; -\varphi_8; \varphi_{10}]$ must hold, it follows from (3) and (4) that

$$6j_1 + 3j_2 - j_3 = 0, \quad 6j_7 + 3j_8 - j_9 = 0. \tag{5}$$

Collecting the coefficients of the transport rates into the vector $\mathbf{q} = [6; 3; -1]$, conditions (5) can be reformulated in terms of orthogonality between pairs of vectors, i.e.,

$$\mathbf{q}^T\mathbf{j}^n = \mathbf{q}^T\mathbf{j}^a = 0, \tag{6}$$

**Table 3** Transport fluxes from extracellular space (ECS) to neuron (n) or astrocyte (a)

| Neuron | | Astrocyte | |
|---|---|---|---|
| Transport | Stoichiometry | Transport | Stoichiometry |
| $j_1 : \mathrm{Glc_{ECS}} \to \mathrm{Glc_n}$ | $j_1 = \varphi_1$ | $j_7 : \mathrm{Glc_{ECS}} \to \mathrm{Glc_a}$ | $j_7 = \varphi_7$ |
| $j_2 : \mathrm{Lac_{ECS}} \to \mathrm{Lac_n}$ | $j_2 = -\varphi_2$ | $j_8 : \mathrm{Lac_{ECS}} \to \mathrm{Lac_a}$ | $j_8 = -\varphi_8$ |
| $j_3 : \mathrm{O_{2,ECS}} \to \mathrm{O_{2,n}}$ | $j_3 = \varphi_4$ | $j_9 : \mathrm{O_{2,ECS}} \to \mathrm{O_{2,a}}$ | $j_9 = \varphi_{10}$ |
| $j_4 : \mathrm{CO_{2,ECS}} \to \mathrm{CO_{2,n}}$ | $j_4 = -3\,\varphi_3$ | $j_{10} : \mathrm{CO_{2,ECS}} \to \mathrm{CO_{2,a}}$ | $j_{10} = -3\,\varphi_9$ |
| $j_5 : \mathrm{Glu_{ECS}} \to \mathrm{Glu_n}$ | $j_5 = -\varphi_5$ | $j_{11} : \mathrm{Glu_{ECS}} \to \mathrm{Glu_a}$ | $j_{11} = \varphi_{11}$ |
| $j_6 : \mathrm{Gln_{ECS}} \to \mathrm{Gln_n}$ | $j_6 = \varphi_5$ | $j_{12} : \mathrm{Gln_{ECS}} \to \mathrm{Gln_a}$ | $j_{12} = -\varphi_{11}$ |

According to the sign convention, a positive flux is from ECS to the cell. Observe that because of physiological considerations, some of the fluxes are constrained to be positive ($j_1, j_3, j_6, j_7, j_9, j_{11}$), and some negative ($j_4, j_5, j_{10}, j_{12}$). The table includes the stoichiometric connections between the reaction and transport fluxes

where the superscript "T" indicates transposition. It follows from the conservation of flux, $\mathbf{J} = \mathbf{j}^{\mathrm{n}} + \mathbf{j}^{\mathrm{a}}$, that

$$\mathbf{q}^{\mathsf{T}}\mathbf{J} = 0. \tag{7}$$

This implies that the three-vectors $\mathbf{j}^{\mathrm{a}}$, $\mathbf{j}^{\mathrm{n}}$ , and $\mathbf{J} \in \mathbb{R}^3$ belong to the plane orthogonal to the vector $\mathbf{q}$, thus they can be expressed as a linear combination of any two linearly independent vectors $\mathbf{v}_1$ and $\mathbf{v}_2$, orthogonal to $\mathbf{q}$. Assuming that $\mathbf{J}$ is given and writing

$$\frac{1}{2}(\mathbf{j}^{n} - \mathbf{j}^{a}) = \alpha_1\mathbf{v}_1 + \alpha_2\mathbf{v}_2, \tag{8}$$

for some scalars $\alpha_1$ and $\alpha_2$, it follows that the general solution $(\mathbf{j}^{\mathrm{n}}, \mathbf{j}^{\mathrm{a}})$ of (6) can be expressed in the form

$$\mathbf{j}^{\mathrm{n}} = \alpha_1\mathbf{v}_1 + \alpha_2\mathbf{v}_2 + \frac{1}{2}\mathbf{J}, \quad \mathbf{j}^{\mathrm{a}} = -\alpha_1\mathbf{v}_1 - \alpha_2\mathbf{v}_2 + \frac{1}{2}\mathbf{J}. \tag{9}$$

Because the vectors $\mathbf{v}_1$ and $\mathbf{v}_2$ can be chosen arbitrarily in the plane orthogonal to $\mathbf{q}$, we conclude that the present model has two degrees of freedom.

To give an interpretation of the degrees of freedom in metabolic terms, we choose the vectors $\mathbf{v}_1$ and $\mathbf{v}_2$ to be

$$\mathbf{v}_1 = \begin{bmatrix} 1 \\ -2 \\ 0 \end{bmatrix}, \quad \mathbf{v}_2 = \begin{bmatrix} 0 \\ 1/3 \\ 1 \end{bmatrix}.$$

It follows from this choice of the basis vectors and (8) that $\alpha_1$ controls the difference in glucose uptake between neuron and astrocyte, and $\alpha_2$ the difference in oxygen uptake.

So far, no constraints have been imposed on the vectors $\mathbf{j}^n$ and $\mathbf{j}^a$ to guarantee that the system is in a physiologically meaningful state and its activity level is energetically sustainable. At steady state, it is reasonable to assume that glucose and oxygen can only be taken up, not released, by the cells. This is guaranteed if we require the components $j_1$, $j_3$, and $j_7$, $j_9$ to be non-negative,

$$j_1 \geq 0, \quad j_3 \geq 0, \quad j_7 \geq 0, \quad j_9 \geq 0. \tag{10}$$

With our current choice of $\mathbf{v}_1$ and $\mathbf{v}_2$, these conditions translate into constraints for coefficients $\alpha_1$ and $\alpha_2$, namely

$$-\frac{1}{2}J_1 \leq \alpha_1 \leq \frac{1}{2}J_1, \quad -\frac{1}{2}J_3 \leq \alpha_2 \leq \frac{1}{2}J_3.$$

The constraints needed to ensure energetic sustainability will be discussed next.

### 2.2 Energy estimates

To guarantee that the metabolic model is energetically feasible, the ATP production must be sufficient to meet the energetic needs of the cells. The total ATP production rate in neuron,

$$\Phi^{\mathrm{n}}_{\mathrm{ATP}} = 2\,\varphi_1 + \varphi_3 + 5\,\varphi_4 = 2\,\varphi_1 + \frac{16}{3}\varphi_4,$$

which follows from (2), can be expressed in terms of the metabolite transport fluxes as

$$\Phi^{\mathrm{n}}_{\mathrm{ATP}} = 2\,j_1 + \frac{16}{3}\,j_3, \tag{11}$$

and similarly, in astrocyte

$$\Phi^{\mathrm{a}}_{\mathrm{ATP}} = 2\,j_7 + \frac{16}{3}\,j_9. \tag{12}$$

In order for the metabolic state of the neuron to be energetically sustainable, the ATP production needs to be sufficient for both the neuron signaling and the household costs.

Let $V$ denote the steady state neurotransmission activity level of the system, measured in terms of the V-cycle rate,

$$\varphi_5 = \varphi_{11} = V.$$

In addition to neurotransmission and signaling, the cells need energy for other routine tasks, e.g., for maintaining the membrane potentials. We refer to the latter as household energy, and denote it by $H_{\mathrm{n}}$ and $H_{\mathrm{a}}$ in neuron and in astrocyte, respectively.

Rather than increasing the complexity of the model with a detailed description of the underlying electrophysiology, we require that part of the ATP hydrolysis goes towards providing the household energy by imposing that

$$\varphi_6 \geq H_{\mathrm{n}}, \quad \varphi_{12} \geq H_{\mathrm{a}}. \tag{13}$$

To guarantee that the ATP turnover in neuron and astrocyte is enough to maintain the activity level of the system, we require that it meets or exceeds the energetic requirements of the household tasks and neurotransmission, as expressed by the inequalities

$$\Phi^{\mathrm{n}}_{\mathrm{ATP}} \geq E_{\mathrm{n}}\, V + H_{\mathrm{n}}, \quad \Phi^{\mathrm{a}}_{\mathrm{ATP}} \geq E_{\mathrm{a}}\, V + H_{\mathrm{a}}. \tag{14}$$

It follows from the choice of $\mathbf{v}_1$, $\mathbf{v}_2$ and (9) that

$$\mathbf{j}^{\mathrm{n}} = \begin{bmatrix} j_1 \\ j_2 \\ j_3 \end{bmatrix} = \begin{bmatrix} \alpha_1 \\ -2\alpha_1 \\ 0 \end{bmatrix} + \begin{bmatrix} 0 \\ 1/3\alpha_2 \\ \alpha_2 \end{bmatrix} + \frac{1}{2}\begin{bmatrix} J_1 \\ J_2 \\ J_3 \end{bmatrix},$$

and

$$\mathbf{j}^{\mathrm{a}} = \begin{bmatrix} j_7 \\ j_8 \\ j_9 \end{bmatrix} = \begin{bmatrix} -\alpha_1 \\ 2\alpha_1 \\ 0 \end{bmatrix} + \begin{bmatrix} 0 \\ -1/3\alpha_2 \\ -\alpha_2 \end{bmatrix} + \frac{1}{2}\begin{bmatrix} J_1 \\ J_2 \\ J_3 \end{bmatrix}.$$

Substituting the expressions for the components of $\mathbf{j}^n$ and $\mathbf{j}^a$ into (11) and (12) and, further, into (14), we have that

$$2\,\alpha_1 + \frac{16}{3}\,\alpha_2 + J_1 + \frac{8}{3}\,J_3 \geq E_{\mathrm{n}} V + H_{\mathrm{n}},$$

and

$$-2\,\alpha_1 - \frac{16}{3}\,\alpha_2 + J_1 + \frac{8}{3}\,J_3 \geq E_{\mathrm{a}} V + H_{\mathrm{a}},$$

from which we conclude that $\alpha_1$ and $\alpha_2$ must satisfy

$$-\,J_1 - \frac{8}{3}\,J_3 + E_{\mathrm{n}} V + H_{\mathrm{n}} \leq 2\,\alpha_1 + \frac{16}{3}\,\alpha_2 \leq J_1 + \frac{8}{3}\,J_3 - E_{\mathrm{a}} V - H_{\mathrm{a}}. \tag{15}$$

Observe that as $V$ increases, so does the left-most term, while the right-most term decreases. The maximum feasible value for $V$ supported by this model, denoted by $V^*$, is found by equating the left and right terms and solving for $V$. The expression for $V^*$ can be written in the form

$$V^* = \frac{2}{E_{\mathrm{n}} + E_{\mathrm{a}}}\left(J_1 + \frac{8}{3}J_3\right) - \frac{H_{\mathrm{n}} + H_{\mathrm{a}}}{E_{\mathrm{n}} + E_{\mathrm{a}}}$$

$$= \frac{2}{E_{\rm tot}} \left(1 + \frac{8}{3}{\rm OGI}\right) {\rm CMR}_{\rm Glc} - \frac{H_{\rm tot}}{E_{\rm tot}}, \tag{16}$$

where $E_{\rm tot} = E_{\rm n} + E_{\rm a}$ and $H_{\rm tot} = H_{\rm n} + H_{\rm a}$. Since formula (16) assumes that all energy produced is used for signaling and household chores, leaving no room for other energetic expenses, it provides an upper bound for the V-cycle activity, that is, $V \le V^*$.

Moreover, starting from equation (16), we can define a theoretical lower bound for the total glucose oxidation as a function of the V-cycle flux. Let ${\rm CMR}_{\rm Glc(ox)}$ denote the flux of glucose oxidized in the unit, measured as one half of the total TCA cycle activity in the system. A simple algebraic manipulation yields

$${\rm CMR}_{\rm Glc(ox)} = \frac{1}{2}(\varphi_3 + \varphi_9) = \frac{\rm OGI}{6}{\rm CMR}_{\rm Glc},$$

therefore ${\rm CMR}_{\rm Glc(ox)}$ can be expressed in terms of $V^*$ as

$${\rm CMR}_{\rm Glc(ox)} = \gamma\, E_{\rm tot}\, V^* + \gamma\, H_{\rm tot}, \quad \gamma = \frac{\rm OGI}{12 + 32\,{\rm OGI}}. \tag{17}$$

This formula expresses the experimentally established linear dependence of the brain's energy demand on the V-cycle activity, see: Sibson et al. (1998) for rodent data, and Gruetter et al. (2001), Lebon et al. (2002), Shen et al. (1999) for human data; see also further discussion on this topic by Gjedde et al. (2002), Hyder et al. (2006) and Calvetti and Somersalo (2012), where the dependency is addressed in the light of model simulations.

### *2.2.1 Inverse calculations*

From the point of view of the mathematical model, it is of interest to consider the following inverse problem: *estimate the cell-level energetic parameters from measured data, using the relation between* ${\rm CMR}_{\rm Glc(ox)}$ *and the rate of the V-cycle.* In their review article, Shulman et al. (2014) (supplementary material) have collected an extensive sample of data consisting of the neuronal ${\rm CMR}_{\rm Glc(ox)}$ values and the corresponding V-cycle rate. To adapt the data to formula (17) referring to the total rather than the neuronal CMR, an estimate for the astrocytic contribution is needed. Lebon et al. (2002) estimate, based on human data, that the astrocytes contribute ∼15 % to the total oxidative CMR. Values given by Gruetter et al. (2001), also based on human data, lead to an estimate of ∼17 % for the astrocytic contribution. We use an estimate of 15 % for the astrocytic part here. With this correction, the values for both human and rodent data are shown in Fig. 2, along with a bivariate linear regression. The slope and intercept of the regression lines are indicated in the figure.

We use the slope and the intercept of the regression line to estimate the energetic parameters, and we assume that OGI = 5.4, as reported by Gjedde (2007). Denoting

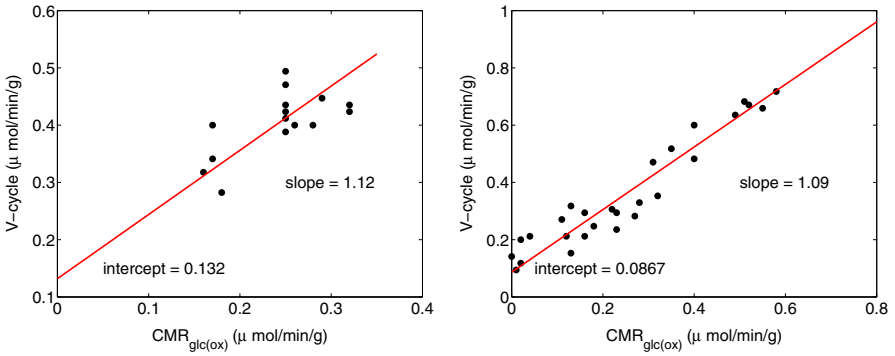


**Fig. 2** The $\mathrm{CMR}_{\mathrm{Glc(ox)}}$ versus V-cycle values with the bivariate regression line. The *left panel* refers to human data, the *right panel* to rodent data. The values come from the supplement of Shulman et al. (2014) with an adjustment to account for the glial contribution, as explained in the text

by $b$ the intercept, we obtain the estimate

$$H_{\mathrm{tot}} = \frac{b}{\gamma}.$$

The estimated values for both human and rodent data are given in Table 4. To find an estimate for the stoichiometric energy cost of the V-cycle, an estimate for $V^*$ is needed. We write

$$V = \theta V^*, \quad 0 < \theta \leq 1,$$

where the upper bound $\theta = 1$ corresponds to a tight energy budget in which all ATP is used either for household or V-cycle activities. Denoting the slope of the linear regression model by $k$, the total energy is given by

$$E_{\mathrm{tot}} = \frac{\theta k}{\gamma}.$$

In Table 4, an estimate based on the data with different values of $\theta$ are given. It is reasonable to assume that the partitioning of the household energy between neuron and glia corresponds to the relative volume fractions. For the partitioning of the energetic need for maintaining the neurotransmission, it is reasonable to take the ratio of CMR of glucose, 85:15, as an estimate, which leads, e.g., for the human brain with $\theta = 1$, to $E_{\mathrm{n}} = 32$ for the neuron and $E_{\mathrm{a}} = 6$ for the astrocyte. The values are close to the ones used by Occhipinti et al. (2010) and Calvetti and Somersalo (2012).

It is of interest to compare the results obtained by this inverse calculations with those given by the "bottom up" approach to cerebral energetic needs first proposed by Attwell and Laughlin (2001), and later updated by Howarth et al. (2012). Attwell and Laughlin (2001) estimate the energy need of the brain by analyzing the basic processes constituting the brain signaling and maintenance. The estimated aggregate amount of ATP molecules required for each glutamate molecule passing through the V-cycle is of the

**Table 4** The estimated values for total household energy and for the stoichiometric energy cost with different values of the ratio $\theta = V/V^*$

| | Human | Rodent |
|---|---|---|
| $H_{\text{tot}}$ | 4.51 | 2.97 |
| $E_{\text{tot}}$ | | |
| $\theta = 1$ | 38 | 37 |
| $\theta = 0.9$ | 35 | 34 |
| $\theta = 0.8$ | 31 | 30 |

The household energy $H_{\text{tot}}$ is given in terms of μmol/min per one gram tissue of ATP dephosphorylation, one mole corresponding to 30.5 kJ of free energy

order of 41 ATP/glutamate, distributed among neurotransmitter recycling (∼3 ATP), postsynaptic processing (∼35 ATP), and presynaptic processing (∼3 ATP). The cost of action potential propagation initially estimated to be around 48 ATP/glutamate, was later downgraded by Howarth et al. (2012) to about one third of the originally proposed value, or 16 ATP/glutamate. These estimates yield a total stoichiometric estimate of $E_{\text{tot}} = 57$. Assuming an OGI of the order of 5–6, the coefficient $\gamma$ ranges in the interval 0.0291–0.0294, leading to an estimate $\gamma E_{\text{tot}}$ ∼1.66–1.68, significantly higher than the estimates obtained here. Part of this difference can be attributed to the model discrepancy, i.e., to the mismatch between the model and reality: the simplified models exclude a number of factors, such as pyruvate carboxylase, glutamate oxidation, or the presence of GABAergic neurons, that have an effect on the in vivo data to which the simplified model is fitted. A detailed discussion, however, is beyond the scope of this work.

### 2.3 Glucose partitioning and lactate flux

It is of interest to interpret the coefficients $\alpha_1$ and $\alpha_2$ in terms of glucose, lactate and oxygen uptake of each cell type. To shed some light on this, we recall that the first components of $\mathbf{j}^{\text{n}}$ and $\mathbf{j}^{\text{a}}$ are the rates of glucose uptake in the corresponding cells, and

$$j_1 = \alpha_1 + \frac{1}{2}J_1, \quad j_7 = -\alpha_1 + \frac{1}{2}J_1,$$

$J_1$ being the total glucose uptake. When $\alpha_1 = 0$, the glucose is evenly partitioned between neuron and astrocyte; a positive $\alpha_1$ shifts the glucose uptake more towards neuron, and a negative $\alpha_1$ towards astrocyte. Similarly, recalling that the third components of $\mathbf{j}^{\text{n}}$ and $\mathbf{j}^{\text{a}}$ correspond to the oxygen uptake of the corresponding cell, and that

$$j_3 = \alpha_2 + \frac{1}{2}J_3, \quad j_9 = -\alpha_2 + \frac{1}{2}J_3,$$

it follows that a large value of $\alpha_2$ corresponds to a highly oxidative neuron, while a large negative $\alpha_2$ shifts the oxidative activity more towards astrocyte. Summarizing, glucose and oxygen partitioning are regulated by $\alpha_1$ and $\alpha_2$, respectively. The lactate partitioning, on the other hand, is a function of both glucose and oxygen partitioning, since

$$j_2 = -2\,\alpha_1 + \frac{1}{3}\alpha_2 + \frac{1}{2}J_2, \quad j_8 = 2\,\alpha_1 - \frac{1}{3}\alpha_2 + \frac{1}{2}J_2.$$

Note that when OGI <6, the neuron–astrocyte complex is a lactate producer because $J_2 < 0$, meaning that lactate is being released. The neuron takes up lactate when $j_2 > 0$, which, in turn, implies that

$$-2\,\alpha_1 + \frac{1}{3}\alpha_2 > -\frac{1}{2}J_2. \tag{18}$$

When this happens, with OGI <6, we have $j_8 < 0$, implying that the astrocyte produces and releases lactate. We refer to this situation as having the system in the ANLS (astrocyte–neuron lactate shuttle) state. Conversely, if $j_8 > 0$, or

$$2\,\alpha_1 - \frac{1}{3}\alpha_2 > -\frac{1}{2}J_2, \tag{19}$$

the astrocyte takes up the lactate produced by the neuron: in this case we say that the system is in NALS (neuron–astrocyte lactate shuttle) state. It is possible that both $j_2$ and $j_8$ are negative, in which case both cells produce lactate.

The direction of the lactate traffic is intimately related to the discussion about the primacy of glucose as the source of energy of neuron, see, e.g., Magistretti et al. (1999), Pellerin et al. (2007), Chih and Roberts (2003). Figure 3 shows how the different choices of $\alpha_1$ and $\alpha_2$ determine whether the system is in NALS, ANLS, or in an in-between state, color coding the different regions of the rectangle representing all possible choices of $(\alpha_1, \alpha_2)$. The energetically feasible area, highlighted in the figure, corresponds to values that satisfy the inequality constraints (15), while the values of $(\alpha_1, \alpha_2)$ for which $V = V^*$ are on the red line across this area. Observe that when $V < V^*$ we implicitly assume that some of the energy produced by the cells is used for unspecified activities other than signaling and household. Alternatively, this can be interpreted as a way to introduce uncertainty in the household energy level. The larger the uncertainty, the wider the feasible region becomes. A particular phenomenon to be pointed out is that when $V$ is close to or equal to $V^*$, hence the feasible region becomes narrow, the direction of the lactate traffic between the cells can be readily deduced from the glucose partitioning, or $\alpha_1$. The central role of glucose partitioning as a control of the net direction of the lactate traffic has been proposed before in the literature, e.g., by Jolivet et al. (2010), Calvetti and Somersalo (2012), Massucci et al. (2013). While the stoichiometry alone cannot answer to the question whether neurons prefer glucose or lactate, the analysis is useful because it shows that, within the framework of the model, fixing glucose partitioning automatically determines the direction of lactate transport. For instance, a 1:1 partitioning with OGI = 5.4 implies

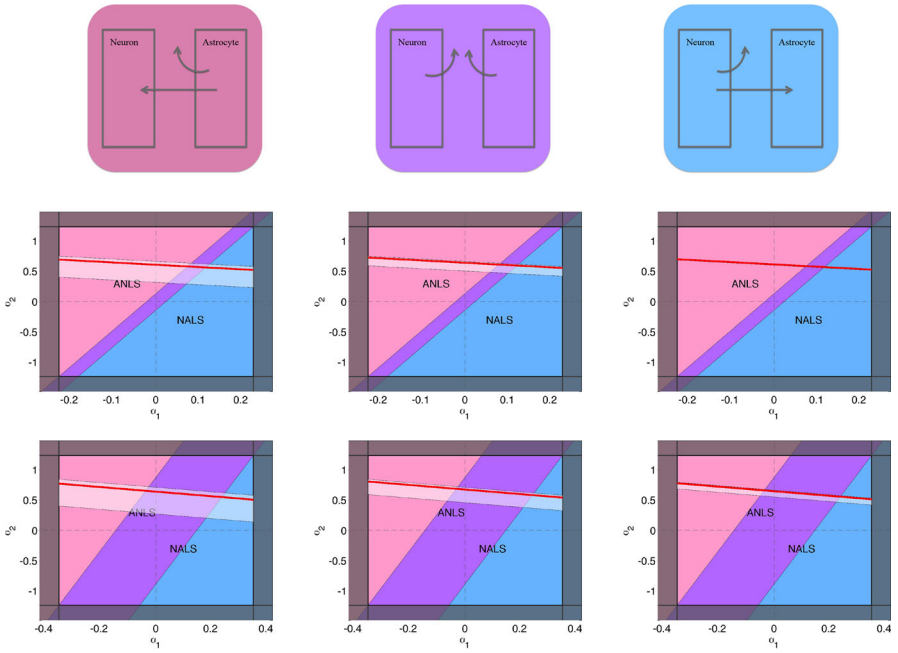


**Fig. 3** *Top row* schematics of the three possible lactate traffic configurations when OGI <6. On the *left*, astrocyte produces lactate, while neuron takes it up (ANLS), in the center, both cells produce lactate, and on the *right*, neuron is the lactate producer and astrocyte oxidizes it (NALS). *Center row* the feasible regions for the parameters $\alpha_1$ and $\alpha_2$ with three different activity levels. In the plots, we use the value OGI $= 5.4$ and $V = 0.25$ μmol/min per one gram tissue. The $\mathrm{CMR}_{\mathrm{Glc(ox)}}$ is computed by using the linear regression model for human data with parameters given in Fig. 2, and the total CMR by $\mathrm{CMR}_{\mathrm{Glc}} = (6/\mathrm{OGI})\mathrm{CMR}_{\mathrm{Glc(ox)}}$. The household energy $H_{\mathrm{tot}} = 4.51$ is divided evenly between the neuron and astrocyte. The *three plots* from *left* to *right* correspond to the total energy values given in Table 4, $E_{\mathrm{tot}} = 31$ (*left*), $E_{\mathrm{tot}} = 35$ (*middle*) and $E_{\mathrm{tot}} = 38$ (*right*). The energy is partitioned between neuron and astrocyte in the ratio 85:15. The *highlighted area* across the field indicates the feasible values of the pair $(\alpha_1, \alpha_2)$ satisfying the inequalities (15). The domain is color coded to indicate whether the pair $(\alpha_1, \alpha_2)$ corresponds to ANLS (*pink*), NALS (*blue*), or if both cells produce lactate (*purple*). The *red line* indicates the values when $V = V^*$. Observe that when the total energy need is lower, the feasible region becomes wider indicating an increased uncertainty due to an unspecified energy expenditure. *Bottom row* to demonstrate the effect of varying OGI, we plot the corresponding feasible regions computed using the same values as for the center row, except for OGI that, to emphasize the effect, we set to the unrealistically low value of OGI $= 3.5$

ANLS, and to argue for NALS, one needs an argument supporting significantly higher glucose uptake by the neuron.

## 3 Multiple units

The model in the previous section was analytically tractable because of the simplified biochemistry and geometry. When working with more complex models, it becomes necessary to employ sophisticated computational techniques, e.g., carrying out a Bayesian flux balance analysis (BFBA) to shed light on possible steady state configurations (Heino et al. 2007, 2010). This approach has been used previously

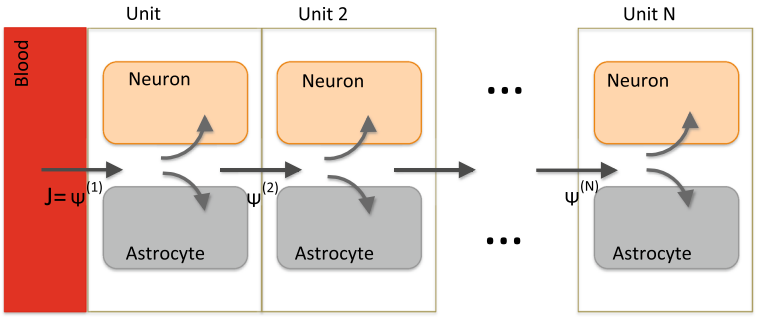


**Fig. 4** A schematic picture of the subunit configuration. The *arrows* indicate the diffusion in the ECS of the tissue, as well as the metabolite uptake by the cell compartments in the units

by the authors to study complex biochemical models for brain metabolism; see, e.g., Occhipinti et al. (2010), Calvetti and Somersalo (2012, 2013). In this work, we extend the analysis towards a geometrically distributed model.

Spatially lumped models with well mixed compartments ignore the effect of diffusion through the tissue. On the other hand, the complex geometric structure of neurons and astrocytes makes a detailed microscopic modeling impossible. Following the idea of bidomain models for myocardium as a response to the same type of modeling challenge (Henriquez 1992), it was suggested by Calvetti et al. (2015) to replace the complex geometric microstructure of the brain tissue by a spatially distributed $n$-domain model, keeping track locally of biochemical compartments of neuron, astrocyte, extracellular space and blood, but allowing diffusion within each compartment. In the cited article, by appropriate model reduction, an idealized spatially distributed one-dimensional model of a Krogh cylinder around a single capillary was derived. The model consists of $N$ identical neuron/astrocyte complexes, communicating with each other through a common extracellular space. We assume that the units are aligned in a one-dimensional array, with the unit $n = 1$ closest to a capillary, the unit $n = N$ most distant from it. A schematic representation of the geometric setting is shown in Fig. 4. Unlike in the previous article (Calvetti et al. 2015), in this work we do not consider the kinetic spatially distributed model, but use the distributed model to demonstrate the uncertainties in the steady state flux balance analysis as a consequence of increased complexity of the model.

### 3.1 Subunit stoichiometry

To set up the model, consider the $k$th neuron–astrocyte unit, $1 \le k \le N$. As in the lumped model, the unit is characterized by the 12 reactions indicated in Fig. 1 and listed in Table 1, and 12 transfers from ECS into the cells, given in Table 3. We collect the transport and reaction fluxes in the vector

$$\mathbf{u}^{(k)} = \begin{bmatrix} \boldsymbol{\varphi}^{(k)} \\ \mathbf{j}^{(k)} \end{bmatrix} \in \mathbb{R}^{24}, \quad \text{where} \quad \boldsymbol{\varphi}^{(k)} \in \mathbb{R}^{12} \quad \mathbf{j}^{(k)} \in \mathbb{R}^{12}.$$

Within each unit, the mass balance conditions define 20 stoichiometric linear equations, listed in Tables 3 and 2, thus defining a stoichiometric matrix $\mathsf{A} \in \mathbb{R}^{20\times 24}$ such that

$$\mathsf{A}\mathbf{u}^{(k)} = 0, \quad 1 \le k \le N. \tag{20}$$

Since each subunit complex is independent, we express the reaction portion of the mass balance equations for all subunits in the aggregate matrix equations,

$$\big(\mathsf{I}_N \otimes \mathsf{A}\big)\mathbf{u} = 0, \quad \mathbf{u} = \begin{bmatrix} \mathbf{u}^{(1)} \\ \vdots \\ \mathbf{u}^{(N)} \end{bmatrix} \in \mathbb{R}^{22N}, \tag{21}$$

where $\mathsf{I}_N$ is the $N \times N$ unit matrix and "$\otimes$" stands for the Kronecker product of the matrices, so that $\mathsf{I}_N \otimes \mathsf{A} \in \mathbb{R}^{20N\times 24N}$.

### 3.2 Coupling subunits by diffusion

Consider next the diffusion. Our model assumes that adjacent units interchange through a diffusion process the four metabolites: glucose, lactate, oxygen, and carbon dioxide. For $k = 1, \cdots, N$, we define the diffusion flux vector,

$$\boldsymbol{\psi}^{(k)} = \begin{bmatrix} \psi_1^{(k)} \\ \psi_2^{(k)} \\ \psi_3^{(k)} \\ \psi_4^{(k)} \end{bmatrix},$$

containing the diffusion fluxes of glucose, lactate, oxygen and carbon dioxide in this order from the ECS of the $(k-1)$th subunit to the ECS of the $k$th subunit, with the convention that $k = 0$ corresponds to the diffusion fluxes from the blood vessel to the first ECS subunit, and $\psi_i^{(k)} > 0$ means net flux towards the $k$th unit, see Fig. 4.

The net flux of metabolites into the $k$th compartment is given by

$$\boldsymbol{\psi}_{\text{net}}^{(k)} = \boldsymbol{\psi}^{(k)} - \boldsymbol{\psi}^{(k+1)}, \quad \boldsymbol{\psi}^{(N+1)} = 0,$$

and to maintain the mass balance in the ECS of each subunit, this net flux must coincide with the uptake/production by the neurons and astrocytes, i.e.,

$$\boldsymbol{\psi}_{\text{net}}^{(k)} = \begin{bmatrix} j_1^{(k)} \\ j_2^{(k)} \\ j_3^{(k)} \\ j_4^{(k)} \end{bmatrix} + \begin{bmatrix} j_7^{(k)} \\ j_8^{(k)} \\ j_9^{(k)} \\ j_{10}^{(k)} \end{bmatrix} = \mathsf{B}\mathbf{u}^{(k)}, \tag{22}$$

where $\mathsf{B} \in \mathbb{R}^{4\times 24}$ is an appropriately defined matrix effectuating the above stoichiometry. To organize these equations into a single matrix equation, define

$$\boldsymbol{\psi} = \begin{bmatrix} \boldsymbol{\psi}^{(1)} \\ \vdots \\ \boldsymbol{\psi}^{(N)} \end{bmatrix} \in \mathbb{R}^{4N},$$

and further,

$$\mathsf{P} = \begin{bmatrix} 1 & -1 & & \\ & 1 & \ddots & \\ & & \ddots & -1 \\ & & & 1 \end{bmatrix} \in \mathbb{R}^{N\times N},$$

so that the system of equations (22) can be arranged into a single matrix equation,

$$\big(\mathsf{P} \otimes \mathsf{I}_4\big)\boldsymbol{\psi} = \big(\mathsf{I}_N \otimes \mathsf{B}\big)\mathbf{u}. \tag{23}$$

Finally, we need to couple the stoichiometric equations to the CMR of the entire unit. We define the net flux vector of glucose, lactate, oxygen, and carbon dioxide from blood to tissue,

$$\mathbf{J} = \begin{bmatrix} J_1 \\ J_2 \\ J_3 \\ J_4 \end{bmatrix},$$

with the convention that a positive sign indicates flux from blood to tissue. We set the boundary condition in matrix form as

$$\mathbf{J} = \boldsymbol{\psi}^{(1)} = \big(\mathbf{e}_1 \otimes \mathsf{I}_4\big)\boldsymbol{\psi}, \quad \mathbf{e}_1 = \begin{bmatrix} 1 & 0 & \cdots & 0 \end{bmatrix} \in \mathbb{R}^{1\times N}. \tag{24}$$

We are now ready to assemble the stoichiometry into a single matrix equation. After defining

$$\mathbf{X} = \begin{bmatrix} \boldsymbol{\psi} \\ \mathbf{u} \end{bmatrix} \in \mathbb{R}^{4N+24N},$$

the stoichiometry is given by the linear system combining equations (21), (23) and (24) as

$$\mathsf{M}\mathbf{X} = \begin{bmatrix} \mathbf{e}_1 \otimes \mathsf{I}_4 & 0 \\ 0 & \mathsf{I}_N \otimes \mathsf{A} \\ \mathsf{P} \otimes \mathsf{I}_4 & -\mathsf{I}_N \otimes \mathsf{B} \end{bmatrix} \mathbf{X} = \begin{bmatrix} \mathbf{J} \\ 0 \end{bmatrix} \in \mathbb{R}^{\mathbf{4+20N+4N}}. \tag{25}$$

The properties of the system matrix $\mathsf{M} \in \mathbb{R}^{(24N+4)\times 28N}$ are analyzed below.

### 3.3 Bound constraints

In addition to the stoichiometry (25), the vector $\mathbf{X}$ has to comply with the a priori bound constraints. In each unit, the reaction fluxes must satisfy the bounds

$$\begin{bmatrix} \varphi_1^{(k)} \\ \varphi_3^{(k)} \\ \varphi_4^{(k)} \\ \varphi_5^{(k)} \end{bmatrix} \ge 0, \quad \begin{bmatrix} \varphi_7^{(k)} \\ \varphi_9^{(k)} \\ \varphi_{10}^{(k)} \\ \varphi_{11}^{(k)} \end{bmatrix} \ge 0, \quad \varphi_6^{(k)} \ge H_{\mathrm{n}}^{(k)}, \quad \varphi_{12}^{(k)} \ge H_{\mathrm{a}}^{(k)},$$

where $H_{\mathrm{n}}^{(k)}$ and $H_{\mathrm{a}}^{(k)}$ are the household energies of the compartments in the $k$th unit. Similarly, the transport fluxes must obey the bound constraints

$$\begin{bmatrix} j_1^{(k)} \\ j_3^{(k)} \\ -j_4^{(k)} \\ -j_5^{(k)} \\ j_6^{(k)} \end{bmatrix} \ge 0, \quad \begin{bmatrix} j_7^{(k)} \\ j_9^{(k)} \\ -j_{10}^{(k)} \\ j_{11}^{(k)} \\ -j_{12}^{(k)} \end{bmatrix} \ge 0.$$

We collet all the conditions into a single matrix inequality,

$$\mathsf{C}\mathbf{X} \ge \mathbf{c}, \quad \mathsf{C} \in \mathbb{R}^{20N \times (4N+24N)}, \tag{26}$$

which is to be understood component-wise.

### 3.4 Degrees of freedom

To analyze the degrees of freedom of the distributed model, we consider the system matrix $\mathsf{M}$ given in (25). The matrix $\mathsf{A} \in \mathbb{R}^{20\times 24}$ is such that $\mathrm{rank}(\mathsf{A}) = 19$ implying that the null space $\mathcal{N}(\mathsf{A})$ has dimension $24 - 19 = 5$. In the light of the single unit analysis, two of the five degrees of freedom can be associated with the glucose and lactate partitioning between neuron and astrocyte, one to the unspecified V-cycle activity, and two to the unspecified ATP demand in each cell. Introducing the notation

$$\mathcal{N}(\mathsf{A}) = \mathrm{span}\{\mathbf{v}_1, \mathbf{v}_2, \mathbf{v}_3, \mathbf{v}_4, \mathbf{v}_5\}, \quad \mathbf{v}_j \in \mathbb{R}^{24}.$$

it follows that if $\mathbf{X}$ is a solution of the system (25), then it must be of the form

$$\mathbf{X} = \begin{bmatrix} \boldsymbol{\psi} \\ \mathbf{u} \end{bmatrix}, \quad \mathbf{u} = \sum_{k=1}^{N} \sum_{j=1}^{5} \alpha_j^{(k)} \mathbf{e}_k \otimes \mathbf{v}_j,$$

where $\mathbf{e}_k \in \mathbb{R}^N$ is the canonical unit basis vector. This follows from the fact that each component $\mathbf{u}^{(k)}$ in (21) needs to satisfy the condition (20). Therefore we have that

$$\big(\mathsf{P} \otimes \mathsf{I}_4\big)\boldsymbol{\psi} = \big(\mathsf{I}_N \otimes \mathsf{B}\big)\mathbf{u} = \begin{bmatrix} \sum_{j=1}^{5} \alpha_j^{(1)} \mathsf{B}\mathbf{v}_j \\ \vdots \\ \sum_{j=1}^{5} \alpha_j^{(N)} \mathsf{B}\mathbf{v}_j \end{bmatrix},$$

which allows us to solve recursively for the diffusion fluxes,

$$\boldsymbol{\psi}^{(\ell)} = \sum_{k=\ell}^{N} \sum_{j=1}^{5} \alpha_j^{(k)} \mathsf{B}\mathbf{v}_j, \quad 1 \le \ell \le N.$$

In particular

$$\mathbf{J} = \boldsymbol{\psi}^{(1)} = \sum_{k=1}^{N} \sum_{j=1}^{5} \alpha_j^{(k)} \mathsf{B}\mathbf{v}_j$$

thus $\mathbf{J} \in \mathsf{B}\big(\mathcal{N}(\mathsf{A})\big)$, a subspace of $\mathbb{R}^4$ which can be shown to be of dimension two. This implies, in particular, that in order for the system to have a solution, the flux $\mathbf{J}$ cannot be assigned arbitrarily, but has only two degrees of freedom. As in the case of a single unit, the two degrees of freedom can be chosen to be $\mathrm{CMR}_{\mathrm{Glc}}$ and OGI, leading to the representation

$$\mathbf{J} = \begin{bmatrix} 1 \\ -2 + \mathrm{OGI}/3 \\ \mathrm{OGI} \\ -\mathrm{OGI} \end{bmatrix} \mathrm{CMR}_{\mathrm{Glc}}, \tag{27}$$

which is in agreement with the stoichiometry of (1).

Based on the considerations above, one would expect the dimension of the null space of $\mathsf{M}$ to be $5N - 2$, with five degrees of freedom coming from each unit, and two lost when assigning the two boundary conditions. Numerical test confirm that this reasoning is indeed correct.

### 3.5 Computational analysis

Summarizing the analysis of the previous sections, the traditional flux balance analysis (see Kauffman et al. 2003) comprises identifying the set of all vectors $\mathbf{X} \in \mathbb{R}^{28N}$ satisfying

$$\mathsf{M}\mathbf{X} = \mathbf{R} = \begin{bmatrix} \mathbf{J} \\ 0 \end{bmatrix} \text{ subject to } \mathsf{C}\mathbf{X} \ge \mathbf{c}, \tag{28}$$

where $\mathbf{J}$ satisfies the condition (27) for some $\mathrm{CMR}_{\mathrm{Glc}} > 0$ and $\mathrm{OGI} > 0$. The solution set is a convex polytope, which can be fully described by its vertices. This is the idea behind the extreme pathway (ExPa) analysis of Schilling et al. (2000) and Papin et al. (2004). An alternative way, advocated by the authors (see, e.g., Heino et al. 2007, 2010) is to explore the solution set by random sampling, generating an ensemble of possible solution vectors that are used to identify particular properties of the solution set. The statistical sampling method of choice is based on Markov Chain Monte Carlo (MCMC) algorithms, and in particular Gibbs sampling and hit-and-run sampling. For examples of different published sampling strategies, see, e.g., Wiback et al. (2004), Massucci et al. (2013).

The approach, referred to as Bayesian flux balance analysis (BFBA), is based on a stochastic extension of the model: the equality constraint in (28) constitutes a basis for a Gaussian likelihood model, that is, $\mathbf{R}$ is treated as an observation with a probability density conditional on $\mathbf{X}$,

$$\mathbf{R} \mid \mathbf{X} \sim \mathcal{N}(\mathsf{M}\mathbf{X}, \Sigma).$$

Here, $\Sigma$ is a symmetric positive definite matrix, which is often chosen to be diagonal. The diagonal entries of $\Sigma$ are the variances of each scalar equation constituting the stoichiometric equations. The interpretation of the stochastic extension therefore is that we do not expect the system to obey strictly the stoichiometry, but allow small variations around the target value. The variance can viewed as encoding uncertainties in the model, due, e.g., to stoichiometric simplifications and approximations, slight deviations from the steady state of the system, or uncertainties in the assumed CMR inputs.

In the Bayesian setting, the bound constraints are interpreted as prior information concerning the unknown $\mathbf{X}$. Denoting by $\Theta$ the multi-dimensional step function that takes on the value one if all the components of the argument are positive and vanishes otherwise, we write

$$\pi_{\mathrm{prior}}(\mathbf{X}) \propto \Theta(\mathsf{C}\mathbf{X} - \mathbf{c}),$$

where "$\propto$" stands for "proportional to". In practice, to obtain a proper prior density, the components need to be restricted further to have their support on some wide interval $[-M, M]$, which is in line with the physiological understanding of the system. By Bayes' formula, the posterior density of $\mathbf{X}$ is then of the form

$$\pi(\mathbf{X} \mid \mathbf{R}) \propto \Theta(\mathsf{C}\mathbf{X} - \mathbf{c}) \exp\left(-\frac{1}{2}(\mathbf{R} - \mathsf{M}\mathbf{X})^{\mathsf{T}} \Sigma^{-1} (\mathbf{R} - \mathsf{M}\mathbf{X})\right).$$

In the described framework it is natural to augment the system with additional information; assuming that we have reasons to believe that a given component $X_j$ is close to a target value, $X_j \approx b_j$, we may simply modify the posterior density by multiplying it with a Gaussian,

$$\pi(\mathbf{X} \mid \mathbf{R}) \to \pi(\mathbf{X} \mid \mathbf{R}) \times \exp\left(-\frac{1}{2w_j^2}(X_j - b_j)^2\right),$$

where $w_j^2$ is the variance determining how stringent the condition is believed to be.

Sampling-based strategies for FBA aim at generating a random sample of vectors that satisfy either exactly or approximately the stoichiometric equations with the prescribed bounds. The MCMC methods generate the sample sequentially through a Markov process so that the vectors are distributed according to the posterior density. In particular, if the sample is denoted by

$$\mathscr{S} = \left\{X^{(1)}, X^{(2)}, \ldots, X^{(N)}\right\},$$

we can compute approximations for expected values with respect to the posterior density, for example

$$\mathsf{E}_{\pi(\mathbf{X}|\mathbf{R})}\left\{f(\mathbf{X})\right\} = \int f(\mathbf{X})\pi(\mathbf{X} \mid \mathbf{R})\mathrm{d}\mathbf{X} \approx \frac{1}{N}\sum_{j=1}^{N} f(\mathbf{X}^{(j)}).$$

For details, see, e.g. Calvetti and Somersalo (2007).

We apply the sampling algorithm to analyze a spatially distributed system that consists of $N = 4$ identical neuron–astrocyte units. In the computation, we assume that each unit has the same household energy need, and that the household energy is distributed between neuron and astrocyte compartments as in the single unit analysis, that is, $H_\mathrm{n} = H_\mathrm{a}$. We run three different tests with the following V-cycle configurations: (1) *baseline stimulation*, in which all four units have the same baseline V-cycle activity $V^{(j)} = V/4$; (2) *proximal activation*, in which the unit $n = 1$ closest to the capillary has the highest V-cycle activity, $V^{(1)} = 0.9\,V$, while the rest of the activity is distributed among the remaining units; and (3) *distal activation*, in which 90 % of the V-cycle activity takes place in the unit $n = 4$ furthest from the capillary. In each case, we generate a sample that, after cleaving off a burn-in sequence of sample vectors identified as non-representative ones, consist of $N = 80{,}000$ sample vectors. The burn-in sequence, identified by visual inspection of the time traces of the components, varies from few thousand (uniform and proximal activation) to about 15,000 (distal activation).

We start by investigating whether the increased number of degrees of freedom changes the conclusions for the lumped model that the lactate trafficking between astrocyte and neuron is determined by the glucose partitioning. The glucose partitioning in the $n$th subunit, the local equivalent of the parameter $\alpha_1$ in the lumped model, is defined as

$$\alpha_1^{(n)} = \frac{\mathrm{CMR}_{\mathrm{Glc,n}}^{n}}{\mathrm{CMR}_{\mathrm{Glc,tot}}^{(n)}}, \quad \mathrm{CMR}_{\mathrm{Glc,tot}}^{(n)} = \mathrm{CMR}_{\mathrm{Glc,n}}^{(n)} + \mathrm{CMR}_{\mathrm{Glc,a}}^{(n)}, \quad 1 \le n \le 4. \quad (29)$$

In the lumped model, the sign of the lactate uptake of the neuron was seen to depend on $\alpha_1$. Figure 5 shows that in the multi-unit geometry, locally such a conclusion is not nec-

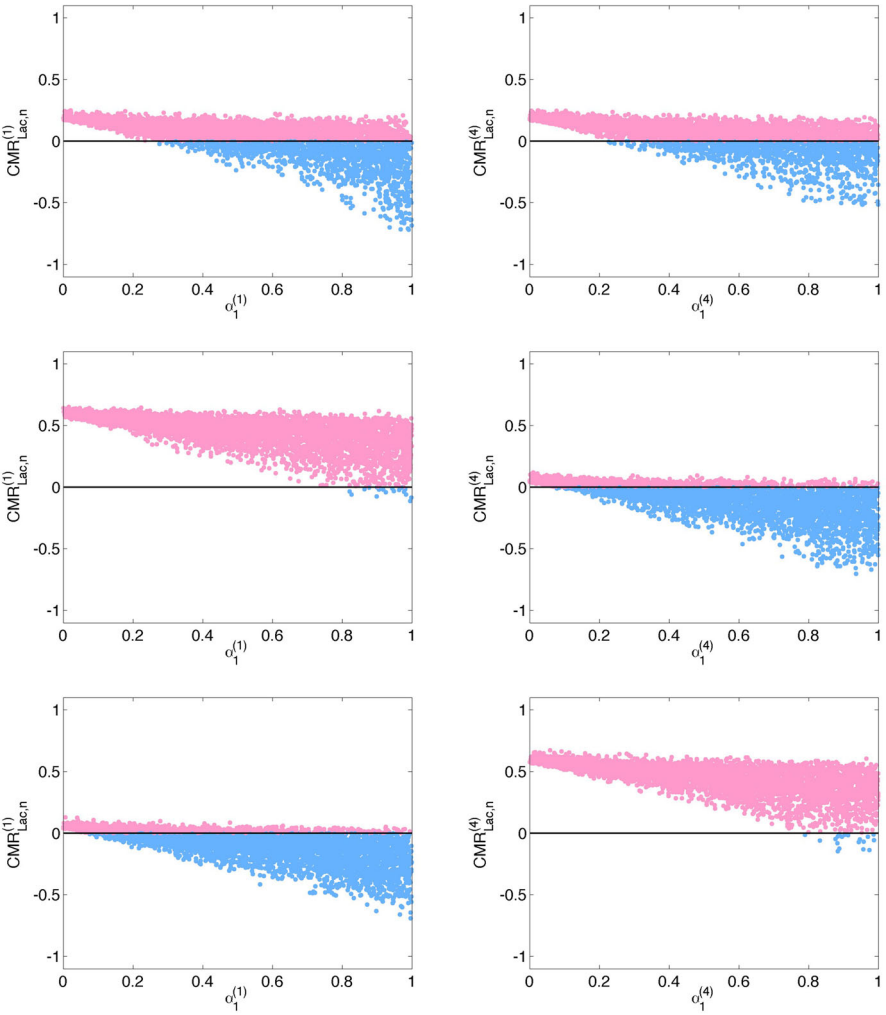


**Fig. 5** Scatter plots of glucose partitioning versus neuronal lactate uptake in individual units. The glucose partitioning is expressed in terms of the ratio of glucose uptake by the neuron in the $n$th unit given in formula (29). The *left column* corresponds to the unit nearest to the capillary, the *right column* to the farthest unit. The rows, from *top to bottom*, correspond to the three different activation protocols: uniform, proximal and distal. The *color coding* indicates whether the neuron is a lactate producer (*blue*) or lactate consumer (*pink*). In the uniform activation protocol, all neurons may be producers or consumers except for the values of $\alpha_1^{(n)}$ closest to zero, when the neuron is deprived from glucose. Both in the proximal and distal activation, the neuron in the active unit is almost certainly taking up lactate

essarily valid: a given value of $\alpha_1^{(n)}$ may correspond both to a neuron producing lactate ($\mathrm{CMR}_{\mathrm{Lac,n}}^{(n)} < 0$) or taking up lactate ($\mathrm{CMR}_{\mathrm{Lac,n}}^{(n)} > 0$). The only exception is the active unit, in which the neuron, due to its elevated energy demand, is almost exclusively a lactate user. The explanation for this behavior is that in the other units, neuron and astrocyte together, may either produce or take up lactate that reaches them by diffusion, and the local relation between neuron and astrocyte becomes more obfuscated.

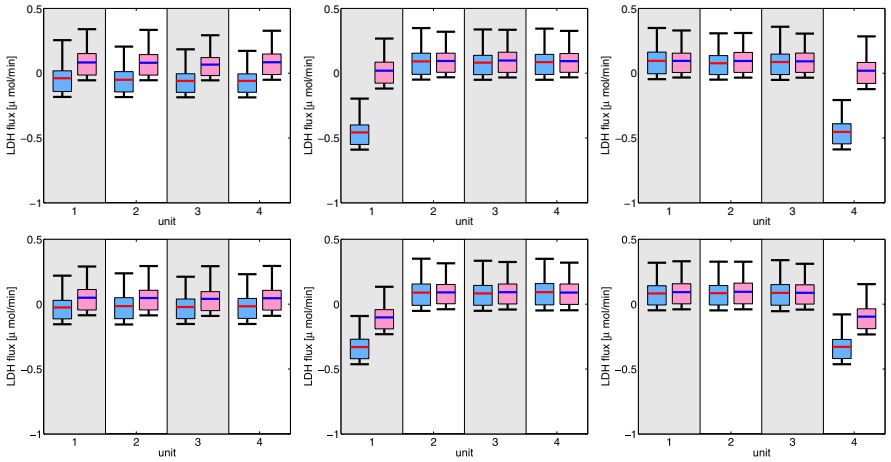


**Fig. 6** *Top row* LDH reaction fluxes in neuron and astrocyte in the five units. The *blue boxes* refer to neurons and the *pink* ones to astrocytes. On the *left*, the V-cycle activity is uniformly distributed among the units, in the *middle*, the active unit is $n = 1$ next to the capillary, on the *right* at the farthest unit $n = 4$. The *boxes* indicate 50 % belief, and the *whiskers* 90 % belief intervals. Observe that in the uniform activation, the neurons are predominantly oxidizing lactate (LDH negative) while the astrocytes produce lactate (LDH positive). In the distal and proximal activations, independently of the location of the high activity, the neuron oxidizes lactate only in the active unit, while in the other units, astrocytes and neurons have a very similar role as lactate producers. *Bottom row* the corresponding *box plots* when the energy partitioning between neuron and astrocyte is more even

To shed some light on which compartments produce or take up lactate, we plot the distribution of the LDH activities in each compartment. Figure 6 summarizes the distributions as box plots, indicating the mean value of the flux over the sample as well as the 50 and 90 % belief intervals computed from the sample. The plot shows that in the case of uniform activation, the neurons favor negative LDH, or lactate oxidation, while in astrocytes, reductive LDH is favored. Interestingly, in the proximal and distal activation protocols, the only compartment oxidizing lactate is the neuron in the most active unit, while all the other units are lactate producers. In particular, the difference between neuron and astrocyte in a non-active unit is minimal.

It is of interest to see to what extent the results depend on the parameters of the model, and in particular, on the partition of the energetic demand between the neuron and the astrocyte. The simulations assume a significantly lower energetic cost (15 %) in astrocyte than in neuron (85 %). For comparison, we reran the sampling algorithm using more evenly distributed energetic costs, assuming that the astrocytic energy demand is 30 % (see Hertz et al. 2007) of the total energy demand. The bottom row of Figure 6 shows the LDH fluxes in the neuron/astrocyte compartments in each unit. As expected, the higher energetic cost in astrocyte in the active unit makes the neuron and the astrocyte more similar, and in terms of the lactate transport, both cells become lactate users (LDH negative), while the inactive units act as lactate producers.

Finally, we plot the distributions of the diffusion fluxes of glucose, lactate and oxygen, see Fig. 7. The fluxes represent the total fluxes between the units, the difference between adjacent fluxes representing the uptake or production of the unit. The glucose

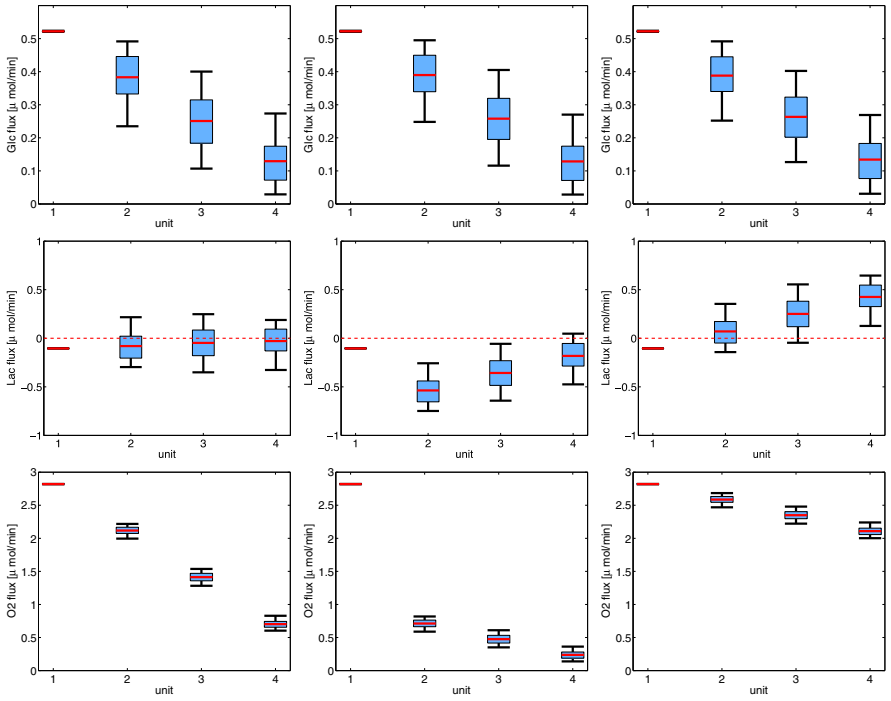


**Fig. 7** The mean diffusion fluxes with 50 % (*box*) and 90 % (*whiskers*) uncertainty intervals. On the *left*, the activation is uniform, in the *middle*, the unit with the highest V-cycle activity is closest to the capillary (Unit 1), while on the *right*, most of the V-cycle activity takes place in the most distant unit (Unit 4). The glucose diffusion (*top row*) is not affected by the location of the activation, while the lactate (*middle*) and oxygen fluxes (*bottom*) are significantly different as the location of the activation changes: in the proximal activation, the units further away from the capillary receive very little oxygen and therefore produce lactate which flows towards the first unit, where the neuron is a net lactate oxidizer. In the distal activation, oxygen flux through the system is high, and lactate is flowing towards the active unit where the neuron takes it up and oxidizes it

diffusion patterns are almost identical regardless of the activation pattern, however, the lactate and oxygen fluxes differ significantly. In the proximal excitation protocol, the neuron in the first unit is highly oxidative and the oxygen flux in tissue decreases significantly. The compartments with low oxygen availability run anaerobic glycolysis, producing lactate that diffuses upwards towards the capillary (negative diffusion flux). In the distal activation, where the highly oxidative neuron is in the last unit, the oxygen diffusion flux is high. However, despite the oxygen availability, the units closer to the capillary run anaerobic glycolysis, thus producing lactate which diffuses towards the active neuron.

## 4 Conclusions

When using mathematical models to support a hypothesis or to explain an observed phenomenon, an important step is to analyze the intrinsic uncertainty of the model,

which can be interpreted as a quantification of the non-uniqueness of the solution. Flux balance analysis can be expressed in the form of a linear system, therefore the non-uniqueness of the solution can be associated naturally with the null space of the system matrix. The problem, however, is usually more complicated due to a number of constraints that are required to guarantee, e.g., that the system is physiologically meaningful and energetically feasible. In this article, a complete analysis of a spatially lumped and biochemically very simplified model is presented, then the discussion is extended to a more complex, spatially distributed model. While the first model admits a fully analytic solution and allows a physiological interpretation of the degrees of freedom, in the second model it was necessary to resort to Monte Carlo sampling to address the high-dimensional null space of the stoichiometric matrix. The point that we want to make with this study is that in spite of the fundamental similarity of the two problems, there are some pitfalls that come with model simplification, in particular, the fact that the increase in the number of degrees of freedom leaves a great deal of space for interpretations that may be conflicting. A remarkable example of such instance is related to the question of the direction of lactate trafficking between neuron and astrocyte. In the framework of a simple lumped model, the direction of lactate flux between neuron and astrocyte can be reduced purely to a question of glucose partitioning, because as far as the energetic needs are concerned, both directions are possible even after fitting the model to measured data. This is in line with literature findings (Jolivet et al. 2010; Nuzzo et al. 2010) acknowledging the central role of glucose partitioning, but coming to opposite conclusions on the direction of the lactate traffic. When the lumped model is replaced by a spatially distributed one, the question about the role of lactate in cerebral energy metabolism becomes much more elusive because the portion of neuron belonging to one compartment may produce and efflux lactate to support energetic need of another part of the neuron, belonging to a different compartment, which takes up lactate to satisfy a higher energetic need. Our results suggest that when simplified models are replaced by more complex ones, which account for phenomena such as diffusion, it is necessary to revisit and reformulate old questions in the new context.

## References

Attwell D, Laughlin SB (2001) An energy budget for signaling in the grey matter of the brain. J Cereb Blood Flow Metab 21:1133–1145

Aubert A, Costalat R (2002) A model of the coupling between brain electrical activity, metabolism and hemodynamics: application to the interpretation of functional neuroimaging. NeuroImage 17:1162–1181

Aubert A, Costalat R (2005) Interaction between astrocytes and neurons studied using a mathematical model of compartmentalized energy metabolism. J Cereb Blood Flow Metab 25:1476–1490

Calvetti D, Cheng Y, Somersalo E (2015) A spatially distributed computational model of brain cellular metabolism. J Theor Biol 376:48–65

Calvetti D, Somersalo E (2007) Introduction to Bayesian Scientific Computing – Ten Lectures on Subjective Computing. Springer Verlag,

Calvetti D, Somersalo E (2011) Dynamic activation model for glutamatergic neurovascular unit. J Theor Biol 264:12–29

Calvetti D, Somersalo E (2012) Ménage à trois: the role of neurotransmitters in the energy metabolism of astrocytes, glutamatergic, and GABAergic neurons. J Cereb Blood Flow Metab 32(2012):1472–1483

Calvetti D, Somersalo E (2013) Quantitative in silico analysis of neurotransmitter pathways under steady state conditions. Frontiers in Endochrinol 4:137
Calvetti D, Somersalo E (2015) Life sciences through mathematical models. Rend Fis Accad Lincei 26(Suppl 2):S193–S201
Chih CP, Roberts EL (2003) Energy Substrates for Neurons During Neural Activity; A Critical Review of the Astrocyte-Neuron Lactate Shuttle Hypothesis. J Cereb Blood Flow Metab 23:1263–1281
Cloutier M, Bolger FB, Lowry JP, Wellstead P (2009) An integrative dynamic model of brain energy metabolism using in vivo neurochemical measurements. J Comput Neurosci 27:391414
Di Nuzzo M, Giove F, Maraviglia B (2010) A biochemical framework for modeling the functional metabolism of the human brain. Biophys Bioeng Letters 2:1–26
Di Nuzzo M, Mangia S, Maraviglia B, Giove F (2010) Changes in glucose uptake rather than lactate shuttle take center stage in subserving neuroenergetics: evidence from mathematical modeling. J Cereb Blood flow Metab 30:586–602
Gjedde A, Marrett S, Vafaee M (2002) Oxidative and nonoxidative metabolism of excited neurons and astrocytes. J Cereb Blood Flow Metab 22:114
Gjedde A (2007) Coupling of brain function to metabolism: Evaluation of energy requirements. In: Lajtha A (ed) Handbook of Neurochemistry and Molecular Neurobiology, 3rd edn. Springer Verlag, Berlin
Gruetter R, Seaquist ER, Ugurbil K (2001) A mathematical model of compartmentalized neurotransmitter metabolism in the human brain. Am J Physiol Endocrinol Metab 281:E100–E112
Harris JJ, Jolivet R, Attwell D (2012) Synaptic energy use and supply. Neuron 75:762–777
Heino J, Tunyan K, Calvetti D, Somersalo E (2007) Bayesian flux balance analysis applied to skeletal muscle metabolic model. J Theor Biol 248:91–110
Heino J, Calvetti D, Somersalo E (2010) Metabolica: a statistical research tool for analyzing metabolic networks. Comput Method Programs Biomed 97:151–167
Henriquez CS (1992) Simulating the electrical behavior of cardiac tissue using the bidomain model. Crit Rev Biomed Eng 21:1–77
Hertz L, Peng L, Dienel GA (2007) Energy metabolism in astrocytes: high rate of oxidative metabolism and spatiotemporal dependence on glycolysis/glycogenolysis. J Cereb Blood Flow Metab 27:21949
Howarth C, Gleeson P, Attwell D (2012) Updated energy budgets for neural computation in the neocortex and cerebellum. Cereb Blood Flow Metab 32:12221232
Hyder F, Patel AB, Gjedde A, Rothman DL, Behar KL, Shulman RG (2006) Neuronal-glial glucose oxidation and glutamatergic-GABAergic function. J Cereb Blood Flow Metab 26:865877
Jolivet R, Allaman I, Pellerin L, Magistretti PJ, Weber B (2010) Comment on recent modeling studies of astrocyte neuron metabolic interactions. J Cereb Blood Flow Metab 30:1982–1986
Kauffman KJ, Prakesh P, Edwards JS (2003) Advances in flux balance analysis. Curr Opin Biotechnol 14:491496
Lebon V, Petersen KF, Cline GW, Shen J, Mason GF, Dufour S, Behar KL, Shulman GI, Rothman DL (2002) Astroglial contribution to brain energy metabolism in humans revealed by 13C nuclear magnetic resonance spectroscopy: elucidation of the dominant pathway for neurotransmitter glutamate repletion and measurement of astrocytic oxidative metabolism. J Neurosci 22:152331
Magistretti PJ, Pellerin L, Rothman DL, Shulman RG (1999) Energy on demand. Science 283:496–497
Massucci FA, Di Nuzzo M, Giove F, Maraviglia B, Castillo IP, Marinari E, De Martino A (2013) Energy metabolism and glutamate-glutamine cycle in the brain: a stoichiometric modeling perspective. BMC Syst Biol 7:103–117
Occhipinti R, Somersalo E, Calvetti D (2010) Energetics of inhibition: insights with a computational model of the human GABAergic neuron-astrocyte cellular complex. Cereb Blood Flow Metab 30:183446
Papin JA, Stelling J, Price ND, Klamt S, Shuster S, Palsson BO (2004) Comparison of network-based pathway analysis methods. Trends Biotechnol 22:400405
Pellerin L, Bouzier Sore AK, Aubert A, Serres S, Merle M, Costalat R, Magistretti PJ (2007) Activity-dependent regulation of energy metabolism by astrocytes: an update. Glia 55:1251–1262
Schilling CH, Letscher D, Palsson BO (2000) Theory for the systemic definition of metabolic pathways and their use in interpreting metabolic function from a pathway-oriented perspective. J Theor Biol 203:229–248
Shen J, Peterson KF, Behar KL, Brown P, Nixon TW, Mason GF, Petroff OA, Shulman GI, Shulman RG, Rothman DL (1999) Determination of the rate of the glutamate/ glutamine cycle in human brain by in vivo 13C NMR. Proc Natl Acad Sci USA 96:823540

Shulman RG, Hyder F, Rothman DL (2014) Insights from neuroenergetics into the interpretation of functional neuroimaging: an alternative empirical model for studying the brain's support of behavior. J Cerb Blood Flow Metab 34:1721–1735

Sibson NR, Dhankhar A, Mason GF, Rothman DL, Behar KL, Shulman RG (1998) Stoichiometric coupling of brain glucose metabolism and glutamatergic neuronal activity. Proc Natl Acad Sci USA 95:316321

Simpson IA, Carruthers A, Vannucci SJ (2007) Supply and demand in cerebral energy metabolism: the role of nutrient transporters. J Cereb Blood Flow Metab 27:176691

Somersalo E, Cheng Y, Calvetti D (2012) The metabolism of neurons and astrocytes through mathematical models. Ann Biomed Eng 40:2328–2344

Wiback SJ, Famili I, Greenberg HJ, Palsson BO (2004) Monte Carlo sampling can be used to determine the size and shape of the steady-state flux space. J Theor Biol 228:437–447